THE JOURNAL OF PHYSICAL CHEMISTRY B

Article

pubs.acs.org/JPCB

Interactions between Grafted Cationic Dendrimers and Anionic Bilayer Membranes

Thomas Lewis

Department of Chemical Engineering, University of Texas at Austin, Austin, Texas 78712, United States

Venkat Ganesan*

Department of Chemical Engineering and Institute for Computational and Engineering Sciences, University of Texas at Austin, Austin, Texas 78712, United States

ABSTRACT: We use polymer self-consistent field theory to study the physics involved in the permeation of charged dendrimer molecules across anionic lipid bilayer membranes. We specifically examine the influence of dendrimer shape deformations, neutral grafts, and pH conditions on the interactions between dendrimers and membranes. Our results indicate that the ability of the dendrimer to undergo conformational rearrangements plays a crucial role in influencing the interactions between the dendrimer and the membrane. At neutral pH, we observe that dendrimers with grafted chains are repelled by the anionic bilayers. However, decreasing the solution pH to endosomal conditions results in attractive dendrimer−membrane interactions under some parametric conditions. We observe that dendrimer insertion into the membrane results in a decreased value in membrane tension at which rupture occurs and, furthermore, that the rupture tension decreases with the addition of grafts to the dendrimer. Our results suggest that dendrimers grafted with neutral polymers can serve as effective pH sensitive delivery vectors.

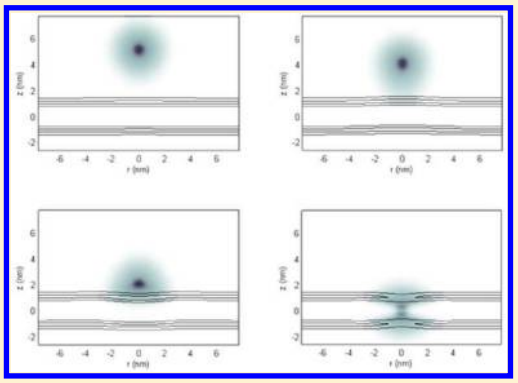

I. INTRODUCTION

Cationic dendrimers have shown great promise in drug and gene therapy applications. For instance, water-soluble dendrimers have been shown to effectively bind to many hydrophobic drug molecules, thus increasing the aqueous solubility of the latter.[1] Cationic dendrimers have also been demonstrated to bind to negatively charged genetic material, which serves the dual purpose of shielding the latter from degradative enzymes in the blood and creating more favorable electrostatic interactions between the nucleic acid material and the negatively charged cellular membrane.[2,3]

Despite the advantages realized through positively charged dendrimers, a number of studies have noted that the nonspecific electrostatic binding to charged lipid head groups of cellular membranes may contribute to dendrimer cytotoxicity, and such effects have been noted to increase with dendrimer size, charge density, and concentration.[4−7] In order to reduce the cytoxicities of dendrimers, researchers have pursued the strategy of lowering the dendrimer surface charges by replacing the surface primary amine groups with noncharged moieties, such as acetyl groups or polyethylene glycol (PEG) chains.[3,8,9] These modifications have been shown to reduce the formation of membrane pores and dendrimer cytotoxicity.[3,8,9]

Despite a number of efforts,[3−20] there is still not full clarity on the physics and parameters governing dendrimer−membrane interactions and the role of grafts in modulating such interactions. Many of the previous theoretical and simulation works have used the model of nanoparticles interacting with membranes to deduce conclusions regarding the dendrimers.[21−25] For instance, Ginzburg and Balijepalli used self-consistent field theory (SCFT) to model the nonspecific interactions between spherical nanoparticles and bilayers and found that the resulting morphology was strongly dependent on the nanoparticle−lipid interaction energies.[21] Recent works by Ting and Wang have extended such methodologies to include electrostatic interactions and also have studied the influence of bilayer surface tensions.[22,23] Their work found that it is energetically favorable for tensionless membranes to partially wrap spherical nanoparticles rather than form pores in the bilayer. Furthermore, they observed that the presence of nanoparticles reduces the rupture tension of the membranes. Coarse-grained (CG) molecular dynamics (MD) simulations by Li and Gu examined the adsorption of surface charged nanoparticles on zwitterionic membranes and were able to show that the driving force for the wrapping of the nanoparticle by the membrane was determined by the interplay of electrostatic attractions and bending rigidity of the membrane.[25] A recent dissipative particle dynamics (DPD)

Received: May 29, 2013
Revised: July 16, 2013
Published: July 17, 2013

dx.doi.org/10.1021/jp4053049 | J. Phys. Chem. B 2013, 117, 9806−9820

study by Ding et al. demonstrated that asymmetry in nanoparticle shape and surface modification of nanoparticles can strongly influence their ability to penetrate bilayer membranes.[24]

While the above studies have provided valuable insights into the interactions between nanoparticles and bilayer systems, such models are not capable of explicitly accounting for all the characteristics of dendrimer molecules. Indeed, our own previous studies (and others) have shown that (i) the distribution of monomers within the dendrimer is nonuniform, with the interior region of the dendrimers possessing a significant amount of void space,[26] and that (ii) the dendrimers may exhibit some flexibility and deform to modulate their interactions.[6,10−20,26−31] Motivated by such considerations, recently there have been a number of MD and DPD studies which have explicitly modeled the dendrimer to study their interactions with charged bilayers.[6,10−20] For instance, atomistic MD simulations by Kelly et al. showed that third generation polyamidoamine (PAMAM) dendrimers deformed significantly as they approached and contacted zwitterionic dimyristoylphosphatidylcholine (DMPC) bilayers.[6,13,14] Coarse-grained MD studies by Lee and Larson showed that dendrimer molecules are capable of inserting themselves into the hydrophobic portion of the bilayer so that the charged terminal amine groups can make contact with the charged head groups of both leaflets.[10] A recent study by Tian and Ma used CG MD to examine the interactions between dendrimers and bilayers of varying compositions.[20] They observed that, when cationic dendrimers interacted with asymmetric bilayers (neutral upper leaflet and negatively charged lower leaflet), the dendrimers were able to move some of the negatively charged lipids to the neutral leaflet. Using a DPD simulation approach, Yan and Yu were able to show that increasing bilayer surface tension resulted in enhanced permeation of charged dendrimers.[15,16] Furthermore, they were able to demonstrate that the insertion of dendrimer molecules into bilayer membranes reduced the surface tension at which the membrane ruptures. These results have highlighted the importance of explicitly accounting for the dendrimer conformational degrees of freedom in examining their interactions with bilayers.

Although there have been a few computational studies which have considered non-grafted dendrimer−membrane interactions, we are aware of only one simulation study which has examined the role of polymer grafts on the dendrimer−membrane interactions.[19] Specifically, Lee and Larson observed that adding neutral grafts to the surfaces of dendrimers reduced their membrane permeability by an extent which was correlated to the length of the grafts. While their study clarified some of the mechanisms underlying the reduced cytotoxicity of grafted dendrimers, their results were based upon specific physicochemical conditions and membrane properties. Hence, the interplay of parameters such as solution pH and membrane tension with the influence of grafts remains unresolved.

Motivated by the above considerations, in this study, we develop a coarse-grained model of grafted, charged dendrimers interacting with anionic membranes. We use such a model to study the following issues:

(i) *How do the dendrimer conformational degrees of freedom influence its interactions with and permeation through membranes?* Since a number of earlier works have shown that dendrimers are capable of deforming in the presence of bilayer membranes,[6,10−20] we undertake a systematic study to clarify the specific influences of dendrimer flexibility and internal voids on the mechanistic pathways underlying dendrimer penetration through membranes.

(ii) *How does the addition of neutral grafts affect the interactions between dendrimers and charged bilayers?* We quantify the free energy of interaction between the dendrimer and membrane as a function of the distance between them, and using such a framework, we examine the influence of dendrimer architecture, such as generation number and graft length, upon the dendrimer−membrane interactions.

(iii) *How do solution pH and membrane surface tension affect the interactions between dendrimers and charged bilayers?* A dendrimer which is outside of the cell and approaching the plasma membrane is exposed to a neutral pH environment, with the bilayer membrane existing in a low tension state. However, once inside the endosome, the pH environment experienced by the dendrimer changes, and the surface tension of the endosomal membrane is speculated to be enhanced through the proton sponge effect.[32−34] Hence, understanding the physicochemical mechanisms underlying the dendrimer−membrane interactions requires knowledge of such features under a variety of membrane tension and pH conditions. Motivated by such issues, we adopt a model which explicitly accounts for acid−base equilibrium effects (a feature lacking in previous works), and thereby quantify the influence of pH conditions. We also examine the influence of membrane tension on the interactions between grafted and non-grafted dendrimers and membranes.

The rest of the article is arranged as follows. In section II, we discuss our SCFT model and the associated terminology. In section III, we present our results, and we conclude with a summary of our findings in section IV.

II. MODEL

A. Self-Consistent Field Theory Model. We consider a single (weakly basic) dendrimer (P) and its grafts (G) in a system containing a lipid bilayer membrane, solvent molecules (S), H^+ and OH^- ions, and monovalent salt ions (denoted as Na^+ and Cl^-). We model the lipids in our system as graft copolymers consisting of a hydrophilic head segment (H) of N_H head monomers, which are attached to two hydrophobic tail segments (T) of N_T tails. Figure 1a presents schematic representations of the lipid and dendrimer molecules in our system. Figure 1b displays a dendrimer (black) with neutral grafted chains (red) attached at the periphery. The zeroth generation of the dendrimer is comprised of the core monomer and the three stemming branches, while the next generation of dendrimers is comprised of the spacers attached at the end groups of the zeroth generation. There are two generational layers attached to the zeroth generation; thus, the generation number, g, of the dendrimer in Figure 1b is $g = 2$. The "functionality", f, of the branches denotes the number of branches stemming from an individual branch point, and in Figure 1b, $f = 3$. In our notation, the number of interior dendrimer monomers, M, comprising the dendrimer molecule is given by

$$M(g) = nf((f-1)^{g+1} - 1) + 1 \quad (1)$$

where n is the number of monomers per spacer. PAMAM dendrimers are composed of both primary amines (NH_2), which reside in the outermost generation, and tertiary amines (NH), which belong to the inner generations.[1] Therefore, the

dx.doi.org/10.1021/jp4053049 | J. Phys. Chem. B 2013, 117, 9806−9820

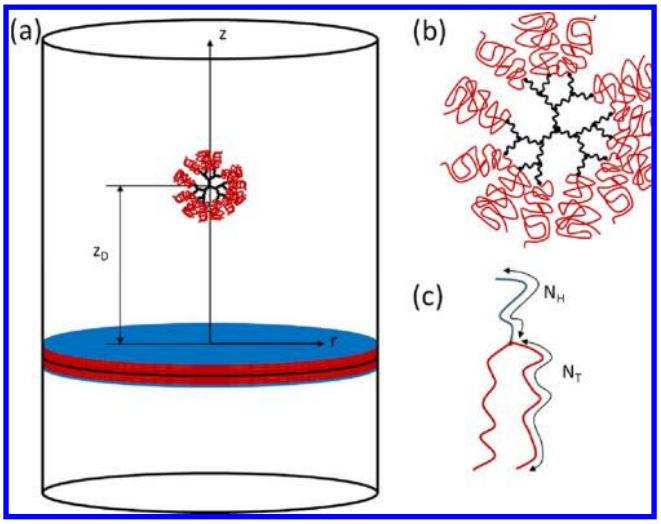

Figure 1. (a) Schematic of our dendrimer−membrane system wherein the dendrimer is separated by distance z_D from the unperturbed bilayer midplane. (b) Schematic of a grafted second generation dendrimer having a functionality of 3. The dendrimer portion is represented in black, while the grafted portions are represented in red. (c) Schematic of a lipid molecule in our system. The head portion is represented in blue, while the tail portions are represented in red.

total number of tertiary amine groups in our dendrimer molecules is given by

$$M_{NH}(g) = f(f-1)^g \tag{2}$$

and the number of tertiary amine groups is given by

$$M_{NH_2}(g) = f((f-1)^g - 1) + 1 \tag{3}$$

We assume that every terminal group of the dendrimer molecule is grafted with a polymer of length N_G such that the number of monomers in the graft portion of the dendrimer molecule is given as

$$M_G(g) = N_G f(f-1)^g \tag{4}$$

We note that, during synthesis of PEG grafted dendrimers, complete PEGylation of the dendrimer primary amines is unlikely to occur.[35,36] Moreover, the addition a PEG chain to a dendrimer converts a primary surface amine to an amide bond, which strongly reduces its ability to absorb a hydrogen ion and thus carry a positive charge. However, to simplify our SCFT framework and the number of parameters involved, we assume that every end group of the dendrimer is PEGylated (cf. Figure 1b) and also allow our surface amine groups to be charged. Therefore, our results compare grafted and non-grafted dendrimers capable of carrying the same amounts of charge, and thus, our results more closely represent comparisons between PEGylated and acetylated dendrimers that have the same number of reacted terminal monomers.

Below, we discuss the assumptions utilized in the derivation of the SCFT equations and present the final expression for the system free energy (see the Appendix for more details of the methodological framework).

(i) We model the dendrimer, neutral grafts, and lipid molecules as flexible continuous Gaussian chains. In reality, the flexibility of these components is dependent upon the chemistry of the monomers.[37] Although previous works have studied the influence of finite dendrimer flexibility and have found it to affect their conformations and density profiles,[38−40] treating both dendrimer and lipid monomers as flexible chains has been shown to still yield qualitatively accurate results.[27−30,41] Therefore, to simplify our model and parameter space, we treat the dendrimer, graft, and lipid molecules as flexible chains.

(ii) We assume that electrostatic interactions are the main *attractive* forces driving the complexation between the dendrimer and membrane molecules. While some simulations have shown that hydrophobic interactions between the dendrimer interior and lipid tail groups may have an important influence on the binding strength between dendrimers and lipid bilayers,[13−15] we neglect such effects in our model to maintain parametric simplicity. The electrostatic interactions in our system are modeled using a classical Coulomb potential[42] with a spatially varying dielectric value, which is assumed to depend linearly on the local component density and dielectric values (see eq 8 below).

(iii) We assume that there are no enthalpic interactions between the dendrimer and its grafts. Some studies have shown that hydrogen bonding between graft chains and dendrimers may occur.[43] However, to reduce the number of parameters, we set the Flory−Huggins interaction parameter between the dendrimer and grafted monomers, χ_{PG}, to be 0.

(iv) We model the total local density of the solvent, dendrimer, graft, and lipid monomers as almost uniform by including a harmonic compressibility penalty for deviations away from the average system density, ρ_0.[42]

(v) We model the charge dissociation of the primary and tertiary amine dendrimer monomers using an approach similar to that adopted by Szleifer et al.[44−46] and Won and co-workers.[47,48] Explicitly, we assume that fractions $\alpha_{P_{NH}}$ and $\alpha_{P_{NH2}}$ of the inner and outermost generation monomers respectively carry dissociable charge groups and are capable of becoming charged through the equilibrium reaction:

$$P_j + H_2O \rightleftharpoons P_jH^+ + OH^- \tag{5}$$

where j represents the NH and NH_2 groups. In a dilute solution containing unconnected dendrimer monomers, the equilibrium fraction of charged monomers, f_b, can be determined through the law of mass action:

$$K_{b,P_j} = \frac{[P_jH^+][OH^-]}{[P_j]} = \frac{f_b \rho_0 \varphi_{OH^-,b}}{1 - f_b} \tag{6}$$

where K_{b,P_j} denotes the equilibrium constant of the dissociation reaction (eq 5), [X] (X ≡ P_j, P_jH^+, OH^-) refers to the concentration in mol/L of species X, ρ_0 is the density of a single monomer, and $\varphi_{OH^-,b}$ is the bulk volume fraction of OH^- ions. The equilibrium constant, K_{b,P_j}, is proportional to exp$(-\beta\Delta G^\circ)$, where $\Delta G^\circ = \mu_{OH^-} + \mu_{P_jH^+} - \mu_{P_j}$ is the free energy of the reaction and μ_i° are the standard chemical potentials of the different species involved in the dissociation reaction. In our calculations, we use different pK_b values for the outermost and inner amine groups.[49] To reduce parametric complexity, we assume that α_{P_j} does not change when comparing grafted and non-grafted dendrimers.

(vi) The lipids used in our system are composed of negatively charged, hydrophilic head groups that are attached to two hydrophobic tail groups. Following the model of Ting and Wang,[22,23] we capture the non-electrostatic energetic interactions of the lipids through the use of both local Flory−

dx.doi.org/10.1021/jp4053049 | J. Phys. Chem. B 2013, 117, 9806−9820

Huggins χ parameters and nonlocal interactions proportional to the square of the local density gradient of the lipid components. As we discuss later in section II.B, we choose the corresponding parameters so that the properties of the bilayers in our system mimic those of experimentally relevant amphiphilic bilayers.[50] We control the surface tension of the lipid bilayers by varying the lipid molecule chemical potentials, μ_L, in addition to the energetic interaction parameters.

Using the above assumptions within a semi-grand-canonical ensemble framework (open with respect to the lipid, solvent, and ion species and closed with respect to the number of dendrimer monomers), we can write the system free energy (within an additive constant) as a functional of the local densities, $\varphi_i(r)$, of the i components (i = S, H^+, OH^-, Na^+, Cl^-, H, T, P_{NH}, P_{NH_2}, and G components) as

$$\begin{aligned}\frac{\beta\mathcal{F}}{\rho_0} = \int d\mathbf{r}\Big[&\sum_{j\neq k}\left(\chi_{jk}\varphi_j\varphi_k + \frac{\kappa_j}{2}[\nabla\varphi_j]^2\right)\\ &+ \sum_{i=\text{ions,S}}\varphi_i(\ln\varphi_i - 1 + \beta\mu_i) + \frac{\zeta}{2}\Big(\sum_l \varphi_i - 1\Big)^2\\ &+ \sum_{j=\text{NH,NH}_2}\alpha_{P_j}\varphi_{P_j}\big[f_j(\ln(f_j) - 1 + \beta\mu_{P_jH^+})\\ &+ (1-f_j)(\ln(1-f_j) - 1 + \beta\mu_{P_j})\big]\\ &+ \Big(\sum_{j=\text{NH,NH}_2} z_{P_jH^+}\alpha_{P_j}f_j\varphi_{P_j} + z_H\alpha_H\varphi_H + \sum_{i=\text{ions}} z_i\varphi_i\Big)\Phi\\ &- \frac{\epsilon}{2\rho_0}|\nabla\Phi|^2\Big] - \frac{V\overline{\varphi}_P}{M}\ln Q_{PG} - \exp(-\beta\mu_L)Q_L\\ &- \int d\mathbf{r}\Big(\sum_{j=\text{NH,NH}_2} w_{P_j}\varphi_{P_j} + w_G\varphi_G + w_H\varphi_H + w_T\varphi_T\Big)\end{aligned} \tag{7}$$

Note that in the above equation the $\mathbf{r}$ dependence is left out for brevity. For the sake of maintaining brevity, we explain the physical meanings of different terms in the above free energy expression in the Appendix. In the above equation, ζ quantifies the strength of the harmonic energy penalty, which is incorporated to reduce total density fluctuations (we consider only volume contributions from the l = P_{NH}, P_{NH_2}, G, S, H, and T species). The parameter f_j represents the local probability that the primary (j = NH_2) and tertiary (j = NH) amine groups exist in a charged state, with z_i denoting the valency of the ith charged species and α_H representing the fraction of lipid head monomers that carry charge. $\Phi(r)$ denotes the electrostatic potential field (normalized by k_BT), with ϵ representing the local dielectric constant (given in units of $\epsilon_0 = 8.85 \times 10^{-12}(A\cdot s)^2/(J\cdot m)$, the permittivity of a vacuum), which is assumed to be given as[22]

$$\begin{aligned}\epsilon(r) = &\epsilon_P\varphi_P(r) + \epsilon_G\varphi_G(r) + \epsilon_H\varphi_H(r) + \epsilon_T\varphi_T(r)\\ &+ \epsilon_S\varphi_S(r)\end{aligned} \tag{8}$$

where ϵ_l represents the dielectric constant of the pure component l. The potential fields, w_i, are Lagrange multipliers conjugate to the respective density fields, $\varphi_i(\mathbf{r})$ (i = P_{NH}, P_{NH_2}, G, H, and T). Q_{PG} and Q_L denote the partition functions for the grafted dendrimer and the lipid molecules in the presence of their respective external potential fields, $w_i(r)$. In order to obtain the system free energy and the density profiles of the system at equilibrium, we minimize the free energy expression (eq 7) with respect the φ_i, w_i, f_i, and Φ fields in the system.[42]

To numerically solve the equations resulting from the above minimization procedure, we employ a cylindrical coordinate system wherein the z-axis of the cylinder is chosen to pass through the center of the dendrimer and is oriented normally to the bilayer membrane (see Figure 1a). We fix the distance between the central dendrimer monomer and the midplane between the two lipid bilayers by enforcing an attractive Gaussian potential on the central dendrimer monomer. We use the lipid and solvent density profiles obtained in the absence of a dendrimer to fix the lipid density profiles at the edge of the cell.

The potential of mean force (PMF) between the dendrimer and membrane quantifies the energy required to move the dendrimer and a membrane to a specified distance from an initial state of infinite separation. By examining the free energy of the dendrimer−membrane system at varying values of the distance between the dendrimer and membrane, we determine how the dendrimer, solution, and membrane tension parameters affect the potentials of mean force (PMFs) between the dendrimer and membrane. A positive PMF value corresponds to a repulsive dendrimer−membrane interaction, while a negative PMF value corresponds to attraction between the dendrimer and membrane.

As discussed in the introduction, there is strong motivation to consider the influence of membrane tensions on the dendrimer−membrane interactions. The tension of a membrane, γ, can be calculated by examining the manner by which the system's equilibrium free energy changes with membrane area for a fixed number of lipid molecules, $\gamma = \partial\mathcal{F}/\partial A|_{n_L}$ (where A is the total area of the membrane bilayer). In order to calculate the surface tension for our system, we calculate the free energy for a 1D canonical ensemble simulation of the lipid components (in the absence of a dendrimer), where the volume fraction of the lipids, $\overline{\varphi}_L$, are fixed and the size of the simulation cell is varied to change the area per lipid headgroup, a. We use such results to map the influence of lipid headgroup area on the resulting surface tension. In turn, by relating the chemical potentials of the lipids, μ_L, to the area per lipid headgroup, we can perform grand-canonical ensemble simulations at specified membrane tensions.

B. Parameters. We fix the functionality and spacer length of the dendrimers to be f = 3 and n = 2, respectively. The dendrimer generation number and grafting lengths in our simulation are varied from g = 3 to g = 4 and N_G = 0 to N_G = 12, respectively. When comparing the results of grafted and non-grafted dendrimers, we use the notation, GXN_GY, to denote a dendrimer having a generation number of X and a grafting length of Y. In line with assumption ii discussed in the previous section, we assume that the Flory−Huggins parameters between the grafted dendrimer (P_{NH}, P_{NH_2}, and G species) and the solvent, lipid components (H and T) are identically zero (i.e., $\chi_{P_jG} = \chi_{P_jH} = \chi_{P_jT} = \chi_{P_jS} = \chi_{GH} = \chi_{GT} = \chi_{GS} = 0$). Furthermore, we set the nonlocal interaction coefficients, κ, for the dendrimer, graft, ion, and solvent species to be 0.

Titration experiments by Niu et al. determined the binding constants for the primary and tertiary amine groups of PAMAM dendrimers,[49] and following their findings, we use $pK_{b,P_{NH_2}} = 4.8$ for the primary and $pK_{b,P_{NH}} = 7.7$ for the tertiary amine groups, respectively. We assume that $\alpha_{PNH} = \alpha_{P_{NH2}} = 0.5$ for the

dx.doi.org/10.1021/jp4053049 | J. Phys. Chem. B 2013, 117, 9806−9820

dendrimer monomers such that only a single monomer per dendrimer branch may be charged. All the solvent and monomer species in our system have a volume of $b^3 = \rho_0^{-1}$, where b = 0.4 nm is the Kuhn segment length of both the dendrimer and lipid species.

We fix the number of lipid head monomers to be $N_H = 2$ and the number of lipid tail groups per chain to be $N_T = 8$. Using these architectural parameters, the total volume of a single lipid is found to be 1.152 nm^3, which agrees with previous observations of hydrated bilayers.[50] The surface charge density of lipid bilayers is a function of their composition, and for biologically relevant membranes, there is a net negative charge in the membrane bilayer. Following the model of Ting and Wang,[22] we fix the fraction of lipid head groups that carry charge, α_H, to be 0.25. The lipid Flory–Huggins and nonlocal square gradient interaction parameters were chosen to be χ_{HT} = 6.0, χ_{TS} = 2.0, χ_{HS} = 0.0, and $\kappa_H = \kappa_T$ = 0.5, respectively. In order to mimic biologically relevant conditions, we fix the salt concentration in the system to be 150 mM. Following the work of Ting and Wang,[22] we choose the dielectric constants for our various components to be ϵ_S = 80, $\epsilon_H = \epsilon_P = \epsilon_G$ = 50, and ϵ_T = 2.

Using the above parameters, we observe tensionless bilayer formation with a corresponding area per lipid molecule, a, equal to 0.67 nm^{-2} and bilayer width of approximately 3.1 nm (cf. Figure 2a), which is in reasonable agreement with previous observations.[50] The surface tension of our membrane as a function of a and the corresponding free energy per lipid are shown in Figure 2b and its inset, respectively. We observe that, at low a, the membrane has negative surface tension values, and under these conditions, an unconstrained membrane would increase its area until a state of zero surface tension is realized. The *rupture tension*, γ_r, of a membrane is the maximum tension a membrane can sustain, beyond which the membrane experiences mechanical failure and the membrane surface tension decreases with increasing a. Here we see that our membrane has a rupture tension of 3.03 k_BT/nm^2 at a = 1.21 nm^2. Quantitatively, we observe that our membrane system mimics the area per lipid headgroup (0.72 nm^{-2}) and rupture tension values (0.75–2.75 k_BT/nm^2) as seen in experiments.[50,51]

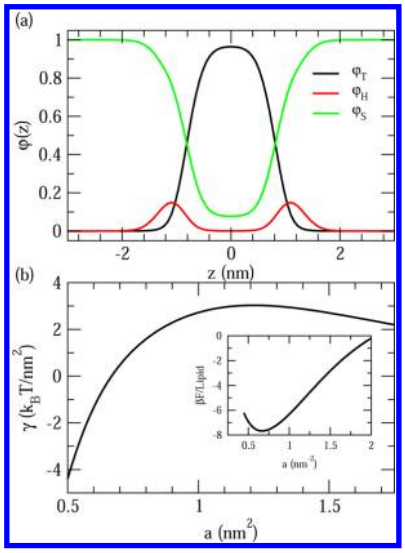

Figure 2. (a) Volume fraction profiles for the solvent and lipid components of our model membrane under zero surface tension. (b) The membrane surface tension, γ (k_BT/nm^2), as a function of the area per lipid headgroup (nm^{-2}). The inset displays the free energy per lipid headgroup as a function of the area per lipid.

III. RESULTS

We begin by examining the interactions between *non-grafted* G3 and G4 dendrimers and a tensionless membrane and compare our results to previous works. Moreover, by using simple variants of our model, we specifically clarify the roles of flexibility and porosity of the dendrimers in influencing their interactions with membranes. Subsequently, we present results which clarify the influence of neutral grafted chains on the interactions between weakly basic dendrimers and charged bilayer membranes. Lastly, we quantify the influence of solution pH and membrane surface tension on the potentials of mean force between the grafted dendrimers and the lipid bilayers.

A. Dendrimer–Membrane Interaction. As a first step to understanding the role of dendrimer architecture and solution conditions upon the dendrimer–membrane interactions, we present some general qualitative features of the dendrimer–membrane interactions seen in our model. In Figure 3, we display the conformations of non-grafted G3 dendrimers in a pH 7 solution for varying distances, z_D, between the dendrimer and a tensionless membrane. As the dendrimer approaches the lipid membrane, it is seen to elongate in the z direction and initiate contact with the negatively charged lipid headgroup monomers (represented through the solid contour lines). Interestingly, we observe only minor deformations in the shape of the bilayer membranes during the approach of the dendrimer. After initiating contact with the membrane, the dendrimer is seen to spread over the bilayer, and in Figure 3e, we explicitly see a branch of the dendrimer reach across the bilayer to initiate contact with the bottom leaflet of the bilayer. Finally, when the dendrimer center is placed at the center of the membrane, we observe a symmetric conformation, wherein the dendrimer initiates contact with both leaflets so that it can maximize the contact between the negatively charged head groups and the positively charged terminal amine groups.

While Figure 3 presents a qualitative picture of the density profiles, in the following, we quantify the shape and nature of the distortions undergone by a dendrimer. For this purpose, we use the gyration tensor, **G**, whose elements are given by

$$G_{ij} = \frac{\int dV(\varphi_{P_{NH}}(\mathbf{r}) + \varphi_{P_{NH_2}}(\mathbf{r}))r_i r_j}{\int dV(\varphi_{P_{NH}}(\mathbf{r}) + \varphi_{P_{NH_2}}(\mathbf{r}))} \quad (9)$$

where r_i is the ith Cartesian coordinate of the position vector, **r**, the origin of which is chosen to be the dendrimer center of mass. Since we operate in a cylindrical system with angular symmetry, the nondiagonal elements of **G** are zero, and $G_{xx} = G_{yy}$. To quantify the nature and magnitude of the dendrimer deformations, we utilize the asphericity parameter

$$A_s = 1 - 3\frac{G_{xx}G_{yy} + G_{xx}G_{zz} + G_{yy}G_{zz}}{(G_{xx} + G_{yy} + G_{zz})^2} \quad (10)$$

and the dendrimer radius of gyration, R,

$$R^2 = G_{xx} + G_{yy} + G_{zz} \quad (11)$$

In Figure 4, we display the dendrimer asphericity and radius of gyrations for G3 and G4 dendrimers as a function of the

dx.doi.org/10.1021/jp4053049 | J. Phys. Chem. B 2013, 117, 9806–9820

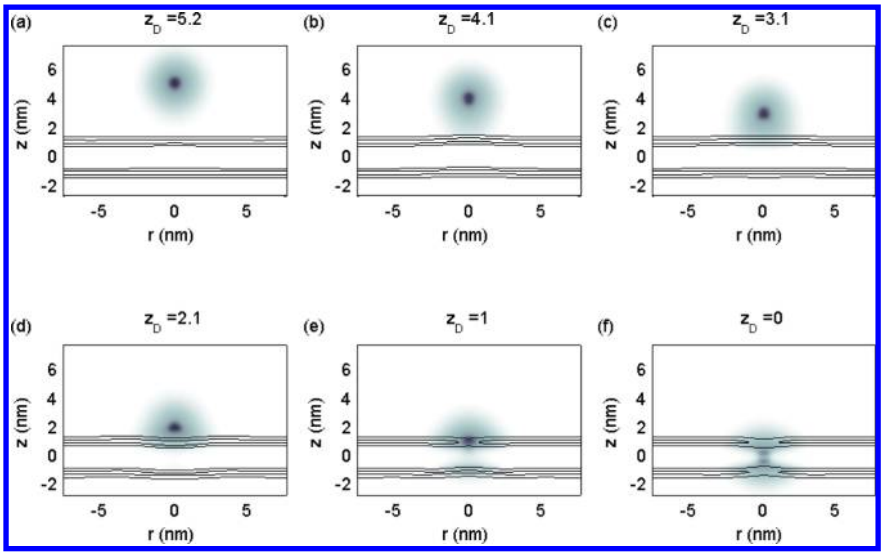

Figure 3. Color plots displaying the volume fraction values of G3 dendrimers, $\varphi_P(r, z)$, in a pH 7 solution at varying distances from the center of the lipid bilayer, z_D. The lipid bilayer headgroup volume fraction values are shown through the contour lines, which correspond to values of $\varphi_H = 0.07$ and $\varphi_H = 0.14$.

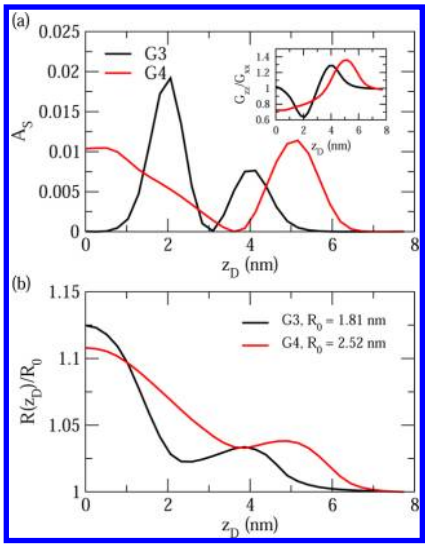

Figure 4. (a) Asphericity of the dendrimer molecules as a function of z_D. The inset displays the ratio G_{zz}/G_{xx}. (b) The radius of gyration of the dendrimer molecule (normalized to its unperturbed value, R_0) as a function of z_D.

distance between the dendrimer and membrane, z_D. For both G3 and G4 dendrimers, we notice that, as the dendrimer approaches a distance of approximately $2R_0$ from the membrane (where R_0 represents the unperturbed size of the dendrimer and corresponds to 4.1 nm for G3 dendrimers and 5 nm for G4 dendrimers), distortions begin to manifest. If we examine the ratio, G_{zz}/G_{xx} (inset of Figure 4a), we see $G_{zz}/G_{xx} > 1$ before the dendrimer initiates contact with the membrane, which is consistent with the prolate spheroidal shapes seen in Figure 3b. Upon initial contact with the membrane (at approximately 3.1 nm for G3 dendrimers and 3.6 nm for G4 dendrimers), we see that the elongation of the dendrimer along the z-axis ceases, and the dendrimer returns to having a nearly spherical shape (cf. Figure 3c), corresponding to $A_S \simeq 0$. During dendrimer insertion into the membrane, we notice that the conformational changes depend on the generation of the dendrimer. For the G3 dendrimer, upon insertion into the membrane (at 2.1 nm), the dendrimer asphericity increases to its maximal value, and the conformation assumes a highly oblate shape (cf. inset of Figure 4a). Interestingly, as the dendrimer moves further into the membrane, we observe a reduction in asphericity, which we attribute to elongations along both the z-axis and the radial direction. As a corroboration of the latter, in Figure 4b, we observe that the size R of the G3 dendrimer does indeed increase when it is inserted inside of the membrane. On the other hand, we notice a different behavior in the A_S and G_{zz}/G_{xx} values for the G4 dendrimers as they penetrate the membrane. Specifically, we see that the asphericity of the G4 dendrimer monotonically increases toward the center of the bilayer membrane, which is consistent with the dendrimer assuming a more oblate shape as it penetrates more deeply in the membrane. These differences between the behaviors of G3 and G4 dendrimers can be attributed to the larger diameter of the latter, as a consequence of which they assume more oblate conformations and maximize contact with the bilayer. Correspondingly, the G4 dendrimer radius of gyration is seen to increase, as seen in Figure 4b.

The above-discussed results of our model agree with the qualitative features reported in previous MD simulations and experimental observations.[6,10,13,14,52] In the atomistic MD simulations by Kelly et al.,[6,13,14] they observed elongation of G3 dendrimers as the latter approached DMPC bilayers. Furthermore, contact between a single dendrimer and leaflet bilayers has been previously witnessed in the CG MD simulations by Lee and Larson,[10] and we display some snapshots from their work in Figure 5 to demonstrate qualitative similarities between their work and our results (compare Figure 5a and b and our results in Figure 3d and e). Solid-state NMR studies by Smith et al. have also confirmed the contact between the dendrimer interior components and lipid tail groups.[52] From their findings, they proposed that the dendrimer molecules contact both leaflets of the bilayer in the transfer of the dendrimer across the bilayer. The obtained density profiles in our work support this proposed behavior.

A unique feature of our model is the explicit accounting for the weakly basic nature of the amine groups along our dendrimer backbone and the resulting modulation of

dx.doi.org/10.1021/jp4053049 | J. Phys. Chem. B 2013, 117, 9806−9820

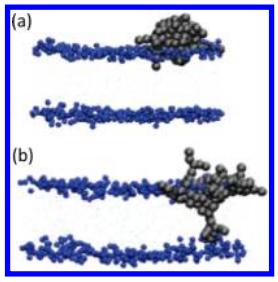

Figure 5. Snapshots of G3 PAMAM dendrimers interacting with a DPPC bilayer after the initial position of 4 nm above the bilayer membrane and 500 ns of simulation time as obtained from the CG MD simulations by Lee and Larson. The black dots represent the dendrimer monomers, while the blue groups represent the DPPC headgroups. Reprinted (adapted) with permission from ref 10. Copyright 2006 American Chemical Society.

dendrimer charges based on the local density of OH^- ions. For instance, in an earlier study, we found that such effects can significantly influence the interactions and complexation of dendrimers with polyelectrolyte molecules.[30] To probe the magnitude of similar effects on our model, we use the quantity ΔQ_P, which is defined as

$$\Delta Q_P = \frac{Q_P(z_D) - Q_{P,0}}{Q_{P,0}} \quad (12)$$

in which $Q_P(z_D)$ is the total charge carried by a dendrimer whose central monomer at z_D and $Q_{P,0}$ is the corresponding charge of the dendrimer far from the membrane. In a nutshell, ΔQ_P quantifies the change in total charge carried by the dendrimer as it approaches the membrane. In Figure 6, we

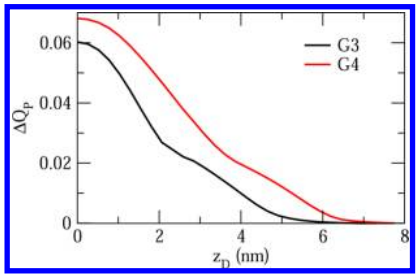

Figure 6. The relative increase in dendrimer charge for a dendrimer at distance z_D from the bilayer as compared to dendrimers in the absence of an anionic membrane, ΔQ_P, as a function of z_D for G3 (black line) and G4 (red line) dendrimers.

display the results for ΔQ_P, wherein we observe a 6−7% increase in the total charge carried by the G3 and G4 dendrimers as they approach the anionic membrane. The negative charge of the lipid head groups of the membranes results in a local depletion of OH^- ions near the lipid head groups, and this in turn *increases* the local dissociation probability, *f*, for the weakly basic dendrimer monomers, thereby increasing the charge carried by the dendrimer. These results suggest that, even when the solution pH is kept constant, the overall charge of the dendrimer can increase by almost 10% to account for the changes in the local ion concentrations. Since previous works have not treated the acid−base equilibrium reaction explicitly, such effects have not been reported in earlier studies.

While the results of Figures 3 and 4 help identify the mechanisms of dendrimer transport through membranes, in order to better quantify the interactions between dendrimers and cells, it is useful to consider the potentials of mean force (PMFs) between the dendrimers and lipid membrane. In Figure 7, we display the PMFs corresponding to non-grafted

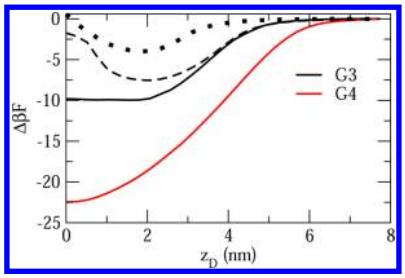

Figure 7. The dendrimer−membrane potential of mean force, $\Delta\beta F$, for a G3 dendrimer (solid black line), *ND*G3 dendrimer (dashed black line), *HS* representing a G3 dendrimer (dotted black line), and G4 dendrimer (solid red line) as a function of distance between the dendrimer core monomer and the bilayer midplane.

G3 and G4 dendrimers as a function of z_D. We observe that the system free energy decreases as the dendrimers approach the lipid bilayer, signifying an attractive interaction between the dendrimer and lipid bilayer. In comparing G3 and G4 dendrimers, we observe that the latter exhibits a deeper and a longer ranged potential well. Such features can be respectively rationalized as a consequence of the larger number of charges and the size of the G4 dendrimers. In physical units, we observe binding strengths of approximately 6.2 kcal/mol at 310 K for our G3 dendrimers. This value is lower than that previously observed by Kelly et al.[13] However, such differences are expected, since we did not account for hydrophobic interactions between the dendrimers and lipid interiors.

The broad and deep potential wells seen in the results of Figure 7 indicate that the dendrimers will experience a strong driving force for binding to the bilayer membrane. However, such an attraction will also serve as a significant barrier for the escape of the dendrimer upon adsorption to the membrane. Thus, passive transport of the dendrimer through a tensionless bilayer into the cellular environment would require very long time scales. Hence, it is not surprising that, even for small dendrimers, active transport (endocytosis) has been suggested as the main mechanism for internalization of dendrimers into the cell.[53]

B. Influence of Dendrimer Flexibility and Porosity. A number of works have considered the model of nanoparticles interacting with membranes, and have observed results qualitatively similar to those discussed in the preceding section.[22] On the basis of such comparisons, one may query what, if any, are the differences in the characteristics of interactions between nanoparticles and dendrimers with membranes. In this regard, we note that our dendrimer model differs from those commonly used for nanoparticles in at least two respects: (i) Our model allows for conformational modulations of the dendrimer molecule (i.e., the dendrimer density profile is not fixed and changes as a function of distance from the membrane). (ii) Our model allows for penetration of the dendrimer by lipid and solvent components (i.e., the dendrimer is porous). Hence, the outstanding questions are, "what are the specific roles played by the flexibility of the dendrimer conformations and the porosity of the dendrimer in influencing its interactions with the membrane?" Below, we

dx.doi.org/10.1021/jp4053049 | J. Phys. Chem. B 2013, 117, 9806−9820

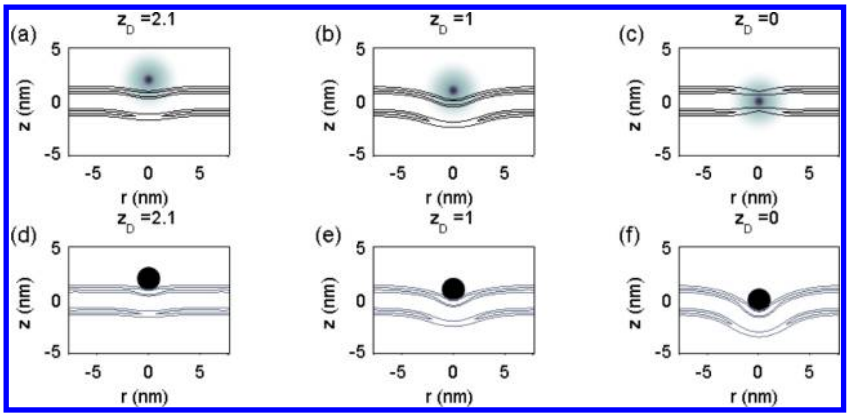

Figure 8. Color plots displaying the volume fraction values of fixed conformation *ND*G3 dendrimers (a–c) and *HS* representing G3 dendrimers (d–f) in a pH 7 solution at varying distances from the center of the lipid bilayer, z_D. The lipid bilayer headgroup volume fraction values are shown through the contour lines, which correspond to values of $\varphi_H = 0.07$ and $\varphi_H = 0.14$.

examine two variants of our model to address the specific roles of such features.

(i) In order to clarify the role of conformational flexibility, we considered a dendrimer of fixed conformation by constraining the density profile of the dendrimer to remain fixed to its conformation far from the membrane. Henceforth, we refer to the G3 dendrimers of fixed conformation as *ND*G3 dendrimers. The corresponding PMF profile for the *ND*G3 dendrimer is displayed by the dashed line in Figure 7. As expected, we see that, at far distances, the PMFs of the deformable G3 (solid black line) and *ND*G3 (dashed black line) dendrimers match. However, at approximately $z_D = 4$ nm (the location at which distortions in the deformable dendrimers manifest, cf. Figure 4a), the PMF profiles begin to differ. Explicitly, we see that the deformable dendrimers exhibit more attractive interactions as compared to the *ND*G3 dendrimers. Interestingly, we observe that the minimum in the dendrimer–membrane PMF profiles for the *ND*G3 dendrimer is offset from $z_D = 0$, indicating that, if the dendrimer conformations are rigidly fixed, there is a barrier to permeation of the dendrimer through our model membrane.

We can better understand the differing trends in the G3 and *ND*G3 dendrimer–membrane PMF profiles by comparing the plots in Figure 3d–f with those of Figure 8a–c, which display the color density plots of the *ND*G3 dendrimer at $z_D = 2.1$, 1.0, and 0 nm, respectively. For the deformable dendrimer, the membrane is observed to be almost unperturbed during the approach of the dendrimer, while the dendrimer itself undergoes significant conformational changes. In contrast, for the case of the *ND*G3 dendrimer, as the dendrimer approaches the membrane, the bilayer is seen to bend substantially in order to initiate dendrimer–membrane electrostatic contacts. Moreover, in the previous section, we saw that the dendrimer deformations allow them to position their charged monomers near the lipid head groups to take advantage of favorable electrostatic interactions. We observe that, while the *ND*G3 dendrimer is also able to insert itself into the membrane to make contact with the leaflets of the bilayer (Figure 8c), the *ND*G3 dendrimer causes more thinning of the membrane as compared to the deformable dendrimer (cf. Figure 3f). The latter can be understood to be a result of the *ND*G3 dendrimer rigidity, which leads to a larger number of dendrimer monomers residing in the hydrophobic region of the bilayer where the lipid density is highest (cf. Figure 2a), resulting in higher steric interactions and membrane thinning. Such effects also incur energetic costs that serve to both reduce the attractive wells of the *ND*G3 dendrimer–membrane PMF profile and create the energetic barrier seen in the insertion of the *ND*G3 dendrimers into the membrane.

Although our *ND*G3 conformations were obtained initially from a highly flexible G3 dendrimer, we believe that the above results may also be used to infer the influence of semiflexibility of the dendrimer bonds on dendrimer–membrane interactions. Indeed, as a crude approximation, the dendrimer with fixed conformations can be considered to be a model for rigid dendrimers. For the highly flexible dendrimers, the conformational rearrangements undergone by the dendrimer are seen to reduce energy barriers for crossing the membrane. In contrast, on the basis of the behavior of the *ND*G3 dendrimer, one may expect that, for a rigid dendrimer, the membrane would distort significantly during the insertion of the dendrimer. Moreover, the PMFs in such cases can also be expected to involve an energy barrier during the permeation of the dendrimer.

(ii) In order to examine the effect of the dendrimer porosity, we considered a model of a hard sphere (HS) whose volume ($V = M(g)/\rho_0$) equaled that of our single G3 dendrimers. For our G3 dendrimers, this corresponded to a hard sphere of radius $R = 1.1$ nm. We assume that the HS contains a uniform distribution of the NH and NH_2 groups and fix the total number of dissociable charge groups to match with our G3 dendrimer.

The results for the HS–membrane PMF are represented in Figure 7 by the black dotted line. Here, we notice that, similar to the *ND*G3 dendrimer, the location of the PMF minimum ($z_D \approx 2$ nm) is offset from the bilayer midplane. More interestingly, the attraction between the HS and membrane is seen to be weaker than that of the *ND*G3 dendrimer. These trends can be rationalized by comparing the morphologies resulting in the *ND*G3 (Figure 8a–c) and HS models (Figure 8d–f). In both cases, we observe that the bilayer begins to deform to initiate contact as the charged dendrimers approach the membrane, which occurs at the cost of an energetic penalty arising from the membrane rigidity. However, we notice an overlap between the dendrimer monomers and the charged lipid head groups in the case of the *ND*G3 dendrimer, whereas, in the case of the HS, there is no possibility for such overlap. Moreover, while the *ND*G3 dendrimer still maintains its ability to insert itself within the membrane, in the case of the HS dendrimer, even for $z_D = 0$, we observe that the membrane has to deform to wrap the HS. Hence, the electrostatic interactions

dx.doi.org/10.1021/jp4053049 | J. Phys. Chem. B 2013, 117, 9806–9820

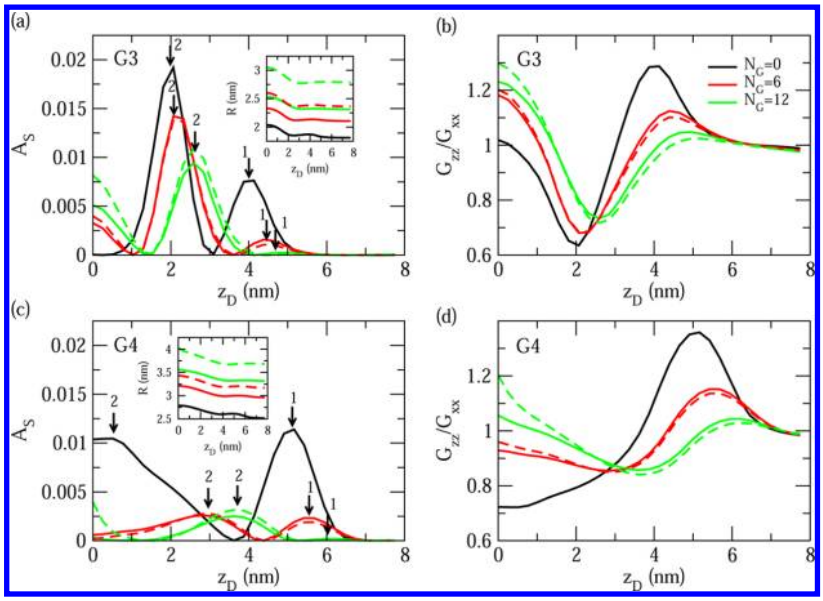

Figure 9. The dendrimer asphericity (a and c) and G_{zz}/G_{xx} ratios (b and d) as a function of z_D for G3 (a and b) and G4 (c and d) dendrimers. The insets quantify the dendrimer radius of gyration values for the G3 and G4 dendrimers as a function of z_D.

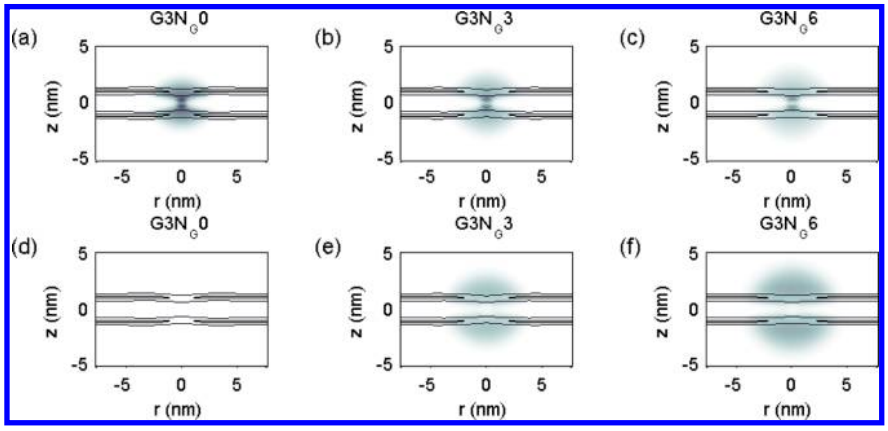

Figure 10. Color plots displaying the volume fraction values of G3 dendrimer interior (a–c) and graft (d–f) monomers in a pH 7 solution at varying values of N_G and separation distance z_D = 0. The lipid bilayer headgroup volume fraction values are shown through the contour lines, which correspond to values of φ_H = 0.07 and φ_H = 0.14.

are expected to be less significant for the HS dendrimer, which is consistent with the observed weaker attractions.

The results presented in this section serve to clarify the influences of dendrimer porosity and flexibility on its interactions with membranes. Overall, both the lipid molecule penetration within dendrimer voids and conformational changes of the dendrimer were seen to play important roles in modulating the energetic interactions between dendrimer and membranes. By choosing a model wherein the volume and charges of the idealized model were chosen to match that of the corresponding flexible dendrimer model, we were able to achieve a more direct and quantitative comparison with the flexible dendrimer model.

C. Effect of Neutral Grafts. As discussed in the Introduction, the addition of neutral PEG grafts to dendrimers has been shown to reduce the cytotoxicities of the latter.[3,8,9] It has been speculated that the presence of grafts reduce the exposed charges of the dendrimer and thereby modulate its interaction with membranes. In this section, we present results quantifying the interactions between grafted dendrimers and membranes to clarify the mechanisms by which grafts influence the permeation processes.

We begin by discussing the influence of grafts on the conformational changes undergone by the dendrimer during its approach and permeation into the dendrimer. We recall our results from section III.A, wherein we observed that the conformational changes of the dendrimer (cf. Figure 3) played a significant role in their interactions with the membrane. In order to quantify the effect of N_G on the dendrimer shapes during permeation, in Figure 9, we present results that quantify the relative shape anistropies (a and c), sizes (a and c insets), and aspect ratios (b and d) of the G3 and G4 dendrimers as a function of z_D for varying N_G values. The solid lines represent the values when only the dendrimer monomer density profiles are considered, while the dashed lines correspond to the conformations of the dendrimer and graft monomers considered together. In Figure 9a and c, we observe that adding grafts to the dendrimer results in a qualitative change in the asphericity profiles for the G3 and G4 dendrimers. Explicitly, we notice that the two maxima present in the *non-grafted* G3 and G4 dendrimers (denoted in the figure as 1 and

dx.doi.org/10.1021/jp4053049 | J. Phys. Chem. B 2013, 117, 9806–9820

2, respectively) are shifted to farther z_D values. Moreover, the magnitude of the maxima for the grafted dendrimers (1 and 2) decreases as N_G is increased. The *shift* to larger z_D for the first two maxima can be attributed to the fact that the presence of the corona from the grafted polymers increases the distance at which the dendrimer "feels" the membrane. The *decrease in the magnitude* of the peaks can be attributed to the fact that the addition of grafts creates results in more steric interactions between the dendrimer and membrane and also shields the electrostatic interactions between the charged dendrimer and lipid monomers. Hence, the dendrimers exhibit less propensity to deform and contact the membrane. Thus, the grafted dendrimers maintain more spherically symmetric conformations.

For smaller values of z_D (when the dendrimer is inside the membrane), we notice in Figure 9a and c that G3 and G4 dendrimers exhibit different trends when N_G is increased. For the G3 dendrimers, the asphericity at small z_D increases with increasing N_G, whereas, for G4 dendrimers, we observe that the A_S values decrease with N_G. To understand these behaviors, in Figure 10, we present color plots for the density values of the (interior) dendrimer (a–c) and (exterior) graft (d–f) monomers for G3 dendrimers of grafting lengths N_G = 0 (non-grafted dendrimer, a and d), N_G = 6 (b and e), and N_G = 12 (c and f) when the dendrimers are located at z_D = 0, which corresponds to the center of the lipid membrane. We observe that adding grafts to the dendrimers causes the latter to stretch in the z direction, which reduces the density of dendrimer monomers that are near the charged lipid monomers. Correspondingly, the corona evident in the density profiles of the grafted material (displayed in Figure 10d–f) is seen to increase in both magnitude and extent.

On the basis of the density profiles displayed in Figure 10, the asphericity trends of G3 dendrimers can be attributed to the increased stretching of the dendrimer along the z-axis (cf. Figures 10a–c and 9b), which results from the steric repulsions between the graft and membrane monomers. By stretching along the z-axis, the dendrimer assumes a conformation which reduces the entropic costs associated with crowding of the grafted chains. To rationalize the behavior of G4 dendrimers, we recall that, in Figure 4a, we demonstrated that the increased asphericity of non-grafted G4 dendrimers relative to non-grafted G3 dendrimers arose from the fact that the charged monomer groups spread out more in the r-direction relative to the z-direction. However, when grafts are attached to the dendrimer, the grafts cause stretching of the dendrimer along the z-axis for the reasons discussed above within the context of G3 dendrimers. The latter is reflected in the decreased A_S values, as seen in Figure 9c, which results in more spherical shapes.

While the above results indicate that the addition of grafts leads to increased steric repulsions, we note that grafts also have an influence upon the electrostatic interactions between the dendrimer monomers and the lipid head groups. To quantify such effects, we use the following measure:

$$Q_{\text{contact}} = \int d\mathbf{r}\Big(\sum_{j=\text{NH},\text{NH}_2} \alpha_{\text{P}_j} f_j(\mathbf{r})\varphi_{\text{P}_j}(\mathbf{r})\Big)\alpha_{\text{H}}\varphi_{\text{H}}(\mathbf{r}) \quad (13)$$

which is proportional to the overlap of the charge densities of the lipid and dendrimer monomers. A small value of Q_{contact} indicates little overlap, whereas a large value corresponds to a high amount of contact between the charged lipid and dendrimer monomers. In Figure 11, we display the Q_{contact} values as a function of z_D for the dendrimers. Not surprisingly,

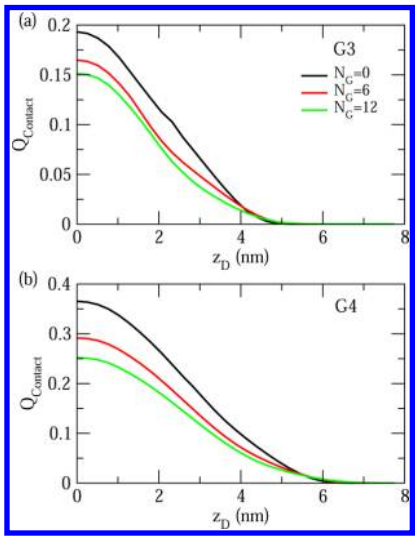

Figure 11. The Q_{contact} values (eq 13) between charged G3 (a) and G4 (b) dendrimer monomers and charged lipid head groups.

we observe higher Q_{contact} values in general for G4 dendrimers which arise as a consequence of the larger number of charged monomers. More interestingly, we observe that increasing the grafting length of the dendrimers reduces the contact between the dendrimer and lipids for all z_D. The latter result validates the hypothesis that the addition of grafted chains to the dendrimer periphery reduces electrostatic contact between the charged dendrimer and lipid headgroup monomers.

The results presented in Figures 9–11 indicate that neutral grafts influence both the steric and electrostatic components of the dendrimer–membrane interactions. As a direct measure of the influence of grafts on the dendrimer–membrane interactions, we present the PMF profiles of G3 and G4 dendrimers as a function of N_G in Figure 12. For both G3 and G4 dendrimers, we observe that the addition of grafts to the dendrimer has a significant effect on the PMFs between the

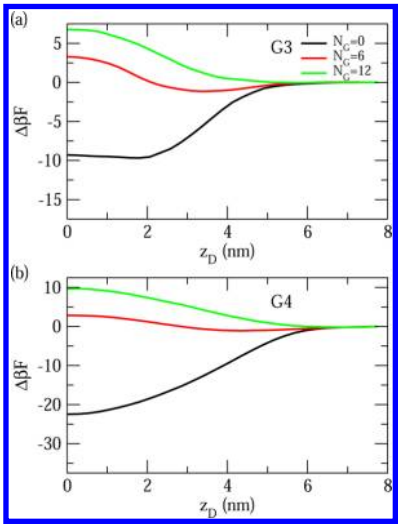

Figure 12. The effect of N_G on the dendrimer–membrane potential of mean force, $\Delta\beta F$, as a function of distance between the dendrimer core monomer and the bilayer midplane for G3 (a) and G4 (b) dendrimers.

dx.doi.org/10.1021/jp4053049 | J. Phys. Chem. B 2013, 117, 9806–9820

dendrimers and charged bilayers. Explicitly, the interactions change from being attractive to becoming repulsive as the dendrimer graft length is increased from $N_G = 0$ to $N_G = 12$. For the intermediate grafting length $N_G = 6$, we observe small regions of attractive interaction when the dendrimer and membrane centers are separated by 3−4 nm. However, this attraction is significantly smaller than the energy barrier required for the dendrimer to penetrate inside of the membrane. Comparing the results of G3 and G4 dendrimers, we observe that they exhibit qualitatively similar trends, with however the range and magnitude of the repulsive barrier being larger for the G4 dendrimers. Such trends can be rationalized by noting that G4 dendrimers are of larger size and also contain larger number of grafts.

In sum, the results presented in this section clarify the effect of neutral grafts on dendrimer−membrane interactions. Explicitly, the presence of grafts was seen to contribute to the steric interactions between the dendrimer and membrane. Moreover, the electrostatic contact between the charged dendrimer and lipid head monomers was also seen to be reduced. The combination of the preceding effects results in a decrease in the magnitude of attraction and introduces a repulsive barrier in the interactions between the dendrimer and the membrane. As a consequence, grafted dendrimers can be expected to exhibit significantly lower propensity for insertion into the membranes, which rationalizes the experimentally reported lower cytotoxicities in such systems.

D. Effect of pH and Membrane Tension. In this final section of our results, we discuss the effects of pH and the membrane tension upon the interaction between dendrimers and anionic membranes. The motivation for such studies comes from the fact that endocytosis of gene delivery vehicles results in their internalization within a lipid endosomic vesicle.[32,33] The pH inside such vesicles is modulated through the addition of H^+ ions by endosomal ATPase. As a consequence of such pH changes, the vesicle osmotic pressure and surface tension of the endosomal membrane increases.[32−34] Hence, it is of interest to understand the influence of pH and membrane tensions on the characteristics of dendrimer−membrane interactions.

Since our model directly incorporates the weakly basic nature of the dendrimer molecules, the modulation of the dendrimer charge arsing from the variation of solution pH is rigorously accounted. To quantify the effect of solution pH on dendrimer−membrane interactions, in Figure 13, we display PMF profiles for the grafted and non-grafted G3 and G4 dendrimers as a function of pH. Overall, we observe that decreasing the solution pH results in a stronger attractive interaction between the dendrimers and the membrane. The latter can be understood to be a result of the enhancement in the total dendrimer charge, Q_P, with decreasing pH (see the insets of Figure 13). Interestingly, our results suggest that the interactions between the N_G6 dendrimers and the membrane can actually switch from being repulsive to becoming attractive as pH is decreased. These results demonstrate that, despite the additional steric interactions brought about by the addition of neutral grafts, the electrostatic interactions between the dendrimer and the lipids may be tuned so as to become dominant at lower pH's to facilitate the insertion of dendrimers into membranes.

To examine the impact of the membrane tension, in Figure 14, we compare the PMF profiles between dendrimers and membranes when $\gamma = 0.0\ k_BT/nm^2$ and $\gamma = 0.74\ k_BT/nm^2$. Interestingly, we witness only minor changes in the

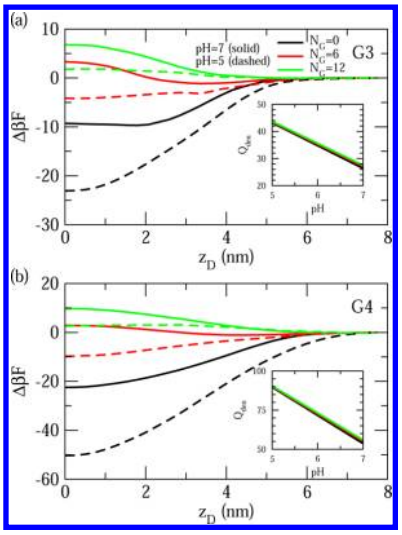

Figure 13. The effect of solution pH on the dendrimer−membrane potential of mean force, $\Delta\beta F$, as a function of distance between the dendrimer core monomer and the bilayer midplane for G3 (a) and G4 (b) dendrimers. The insets quantify the dendrimer charge, Q_{den}, for an individual dendrimer in the absence of a membrane.

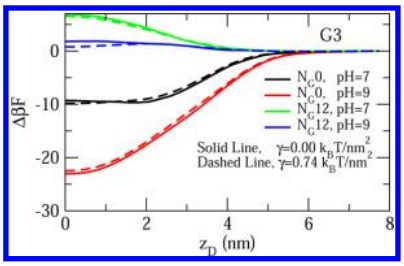

Figure 14. The effect of membrane tension, grafting length, and pH on the potential of mean, $\Delta\beta F$, between G3 dendrimers and an anionic lipid bilayer. Solid lines represent $\gamma = 0.0\ k_BT/nm^2$, while dashed lines represent $\gamma = 0.74\ k_BT/nm^2$.

dendrimer−membrane PMFs upon variation of membrane tensions. Such a behavior contrasts significantly with the results of Ting and Wang in which they observed that the attraction between impenetrable nanoparticles and membranes decreased significantly (potential well depth shifted from $\sim -31k_BT$ to $\sim -21k_BT$ for a G5 dendrimer) when the membrane surface tension increased from $\gamma = 0.0\ k_BT/nm^2$ and $\gamma = 0.74\ k_BT/nm^2$.[22] Since the energetics of nanoparticle interaction with the membrane are influenced by the membrane deformations (see discussion in the context of Figure 8), their results can be straightforwardly understood to be a consequence of the increased energy required to deform the membrane to wrap around the nanoparticle. In contrast, the porosity and flexibility of our dendrimer model significantly reduce the extent to which the membranes deform during dendrimer−membrane insertion (cf. Figure 3). Hence, it is not surprising that the dendrimer−membrane PMF exhibits only a weak dependence on membrane tension.

Previous works have shown that the rupture tension of membranes, γ_r, can be reduced in the presence of dendrimers, and so it is of interest to understand how the addition of grafts to dendrimer molecules affects their ability to modulate the rupture tension. To determine the effect of dendrimer insertion on the membrane rupture tension, we simulate a dendrimer−membrane system with the dendrimer center of mass situated

dx.doi.org/10.1021/jp4053049 | J. Phys. Chem. B 2013, 117, 9806−9820

at $z_D = 0$ for increasing values of membrane surface tension. As we increase γ, we eventually see the formation of a pore which expands indefinitely, and the membrane components in our simulation vanish, which corresponds to the rupture tension of the dendrimer−membrane system.

In Figure 15, we display the rupture tension, γ_r, observed for bilayer membranes in the presence of G3N_G0 and G3N_G12

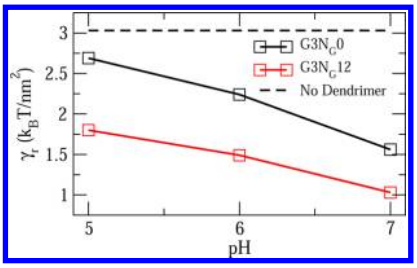

Figure 15. The effect of pH and neutral grafts on the rupture tension, γ_r, of anionic bilayer membranes.

dendrimers as a function of pH. Here we observe that the membrane rupture tensions are uniformly lower in the presence of the dendrimer as compared to the bare membrane ($\gamma = 3.03$ k_BT/nm^2, indicated by the dotted line in Figure 15). The reduction in rupture tension by dendrimers can be understood to be a consequence of dendrimer-induced disruption of lipid arrangement, which is expected to lower the energy barrier for pore formation.[15,16] As the charge on the dendrimer is increased (by decreasing the solution pH), the rupture tension of the membrane is seen to increase. Such an effect has also been previously witnessed in the context of nanoparticles and results from the enhanced adhesion between the charged dendrimer and lipid head monomers resulting from the increased dendrimer charge.[22] However, when grafts are added to the dendrimers, we observe a reduction in the rupture tension. This reduction in rupture tension can be attributed to the decreased dendrimer−membrane adhesion strength which results from the steric repulsions between the grafts and the membrane. Since rupture tension provides a measure for the ease of releasing the gene delivery vehicles, the above results indicate that the addition of grafts may promote the ease with which dendrimers are released from the endosome.

IV. SUMMARY

In this article, we reported results of polymer SCFT calculations which examined the interactions between charged dendrimers (with and without neutral grafts) and anionic lipid bilayer membranes. Our results were in qualitative agreement with observations from previous molecular dynamics simulation studies.[10,13,14] We observed that dendrimers undergo significant conformational changes to maximize contact between their monomers and the negatively charged lipid head groups. By performing corresponding calculations for interactions between membranes and (i) nondeformable, porous dendrimers and (ii) charged hard spheres, we were able to delineate the influences of the penetrability and deformability of the dendrimer on the PMFs for dendrimer−membrane interactions. For flexible dendrimers, there was a strong attraction seen between the dendrimer and membrane, with no energy barriers in the insertion of the dendrimer into the membrane. In contrast, the nondeformable dendrimers and charged hard spheres exhibit an energy barrier with an effective well at a finite distance from the membrane. The dendrimer−membrane attraction was seen to be strongest for the deformable dendrimers and weakest for the charged hard spheres.

The addition of neutral grafts to the dendrimer exterior was shown to affect the attraction between the dendrimer and the membrane. In general, we observed that, at neutral pH, the grafted dendrimers experienced a repulsive dendrimer−membrane potential, which arose from the increase in steric repulsions between the grafts and the membrane. However, when the pH was lowered to 5 (representative of the environment in the endosome), both the G3N_G6 and G4N_G6 dendrimers developed an attractive well in their PMF profiles. Furthermore, the addition of grafts to the dendrimer was seen to reduce the required tension for membrane rupture and release the genetic material.

The results in this work provide perspective on both the general manner through which dendrimers permeate cellular membranes and how neutral grafts affect dendrimer−membrane interactions. When the optimally designed grafted dendrimers are near the cell membrane at physiological pH, they will not insert themselves into the membrane; however, upon internalization, the drop in pH and corresponding protonation of the tertiary amine groups results in favorable dendrimer−membrane interaction. The insertion of the dendrimer into the bilayer in turn reduces the tension required for the endosomal membrane to rupture which helps to release the internalized material.

APPENDIX

In this appendix, we provide the details of our free energy model and the equations resulting from its minimization. Many of the details of our model are identical to what we used in our previous studies.[27−30] In eq 7, we provided the mean field expression for our system free energy. The first term,

$$\sum_{j\neq k}\int d\mathbf{r}\chi_{jk}\varphi_j\varphi_k \tag{14}$$

accounts for nonspecific, pairwise enthalpic interactions, quantified in this work through Flory−Huggins χ parameters.[42] The second term,

$$\sum_{j}\int d\mathbf{r}\frac{\kappa_j}{2}[\nabla\varphi_j]^2 \tag{15}$$

reduces the sharpness of the lipid head tail interface and provides an additional parameter through which we can control the properties of our bilayer membrane.[22] The terms,

$$\begin{aligned}\int d\mathbf{r}\Big(&\sum_{j=\mathrm{NH},\mathrm{NH}_2}\alpha_{\mathrm{P}_j}\varphi_{\mathrm{P}_j}\big[f_j(\ln(f_j)-1+\beta\mu_{\mathrm{P}_j\mathrm{H}^+})\\&+(1-f_j)(\ln(1-f_j)-1+\beta\mu_{\mathrm{P}_j})\big]\\&+\sum_{i=\mathrm{ions,S}}\varphi_i(\ln\varphi_i-1+\beta\mu_i)\Big)\end{aligned} \tag{16}$$

account for the chemical potential, mixing, and translational entropies of the ions, solvent, and the charged/uncharged dendrimer monomers.[44] We reduce fluctuations in our system density through the term[42]

$$\int d\mathbf{r}\frac{\zeta}{2}\Big(\sum_i\varphi_i-1\Big)^2 \tag{17}$$

dx.doi.org/10.1021/jp4053049 | J. Phys. Chem. B 2013, 117, 9806−9820

where ζ represents a measure of the compressibility of the system. We treat all ions in our system explicitly and calculate the electrostatic energy[42] from

$$\int d\mathbf{r}\left[\left(\sum_{j=\mathrm{NH},\mathrm{NH}_2} z_{\mathrm{P}_j\mathrm{H}^+}\alpha_{\mathrm{P}_j}f_j\varphi_{\mathrm{P}_j\mathrm{H}^+} + z_{\mathrm{H}}\alpha_{\mathrm{H}}\varphi_{\mathrm{H}} + \sum_{i=\mathrm{ions}} z_i\varphi_i\right)\Phi - \frac{\epsilon}{2\rho_0}|\nabla\Phi|^2\right] \tag{18}$$

The last terms

$$-\frac{V\overline{\varphi}_{\mathrm{P}}}{M}\ln Q_{\mathrm{PG}} - \exp(-\beta\mu_{\mathrm{L}})Q_{\mathrm{L}} - \int d\mathbf{r}\left(\sum_{j=\mathrm{NH},\mathrm{NH}_2} w_{\mathrm{P}_j}\varphi_{\mathrm{P}_j} + w_{\mathrm{G}}\varphi_{\mathrm{G}} + w_{\mathrm{H}}\varphi_{\mathrm{H}} + w_{\mathrm{T}}\varphi_{\mathrm{T}}\right) \tag{19}$$

account for the conformational entropy of the dendrimer and lipid chains.[42] The terms Q_{PG} and Q_{L} represent the single chain partition functions of the dendrimer and lipid chains. To obtain these partition functions, we assume that the conformations of the grafted dendrimers and lipid molecules can be described using a continuous Gaussian chain model. In such a model, the chain is represented by the continuous contour path, $\mathbf{r}_i(s)$, and the corresponding stretching energy of the chain is given by the general expression,[42]

$$\beta U_0(\mathbf{r}) = \frac{3}{2b^2}\sum_{i=0}^{n_{\mathrm{branch}}}\int_{s_{i,0}}^{s_{i,f}}\left|\frac{d\mathbf{r}_i(s)}{ds}\right|^2 ds \tag{20}$$

where b is the Kuhn segment length of the polymers, n_{branch} is the total number of the respective dendrimer and lipid branches, and $s_{i,0}$ and $s_{i,f}$ are locations of the beginning and ending monomers for the i^{th} branch.

The partition functions, Q_j (j = PG,L), can be determined by calculating the statistical weights of a chain diffusing along its trajectory to a point in space, which are given by $q_j(\mathbf{r}, s)$ and $q_j^\dagger(\mathbf{r}, s)$. The functions $q_j(\mathbf{r}, s)$ are calculated by first starting from s = 0 (center of the dendrimer (j = PG) or lipid headgroup (j = L)) and then moving forward in s. In a similar fashion, $q_j^\dagger(\mathbf{r}, s)$ describes the statistical weight of the chain diffusing backward in s, starting from the $s_{j,end}$ (edge of the grafted dendrimer (j = PG) or free end of the lipid tail group (j = L)). The partition function of grafted dendrimer and lipid chains can then be calculated from:[42]

$$Q_j = \frac{1}{V}\int d\mathbf{r} q_j^\dagger(\mathbf{r}, s = 0) \tag{21}$$

The functions $q_j(\mathbf{r}, s)$ and $q_j^\dagger(\mathbf{r}, s)$ can be found from the following "diffusion-like" equations:[42]

$$\frac{\partial q_j}{\partial s} = \frac{b^2}{6}\nabla^2 q_j - W_j(\mathbf{r}, s)q_j \tag{22}$$

The $W_j(\mathbf{r},s)$ functions are given by

$$W_{\mathrm{PG}}(\mathbf{r}, s) = \begin{cases} w_{\mathrm{P,NH}}(r) & 0 \le s_{\mathrm{PG}} < n(g-1) \\ w_{\mathrm{P,NH}_2}(r) & n(g-1) \le s_{\mathrm{PG}} < ng \\ w_{\mathrm{G}}(r) & ng \le s_{\mathrm{PG}} < ng + N_{\mathrm{G}} \end{cases} \tag{23}$$

and

$$W_{\mathrm{L}}(\mathbf{r}, s) = \begin{cases} w_{\mathrm{H}}(r) & 0 \le s_{\mathrm{L}} < N_{\mathrm{H}} \\ w_{\mathrm{T}}(r) & N_{\mathrm{H}} \le s_{\mathrm{L}} < N_{\mathrm{T}} \end{cases} \tag{24}$$

for the dendrimer and lipid molecules respectively. In order to fix the position of the dendrimer center at $\mathbf{r} = (r = 0, z = z_{\mathrm{D}})$, we apply a Gaussian constraining potential (variance =$0.05R_g$, where $R_g = ((N_{\mathrm{H}} + N_{\mathrm{T}})/6b)^{1/2}$), for the "initial" condition, $q_{\mathrm{PG}}(\mathbf{r}, s = 0)$. For the lipid chains, we apply $q_{\mathrm{L}}(\mathbf{r}, s = 0) = 1$. The function $q_j^\dagger(\mathbf{r}, s)$ that runs from the periphery of the dendrimer is given by

$$-\frac{\partial q_j^\dagger}{\partial s} = \frac{b^2}{6}\nabla^2 q_j^\dagger - W_j(\mathbf{r}, s)q_j^\dagger$$
$$q_j^\dagger(\mathbf{r}, s = s_{\mathrm{end}}) = 1 \tag{25}$$

In order to account for the branching within the dendrimer, we apply the following conditions[54]

$$q_{\mathrm{PG}}^\dagger(\mathbf{r}, s_i^-) = [q_{\mathrm{PG}}^\dagger(\mathbf{r}, s_i^+)]^{f-1}; \quad s \le ng \tag{26}$$

$$q_{\mathrm{PG}}(\mathbf{r}, s_i^+) = q_{\mathrm{PG}}(\mathbf{r}, s_i^-)[q_{\mathrm{PG}}^\dagger(\mathbf{r}, s_i^+)]^{f-2}; \quad s \le ng \tag{27}$$

where $q_{\mathrm{PG}}^\dagger(\mathbf{r}, s_i^-)$ refers to spatially dependent chain propagator for a monomer at a value of s that is infinitesimally smaller than s_i, the value of s at the i^{th} branching point. The above conditions (eqs 26 - 27) embody the fact that at the dendrimer branch points, the $f - 1$ outer generation chains connect. This is analogous to $f - 1$ independent particles diffusing to the same point in space at the exact same time.[54] In a similar fashion, for the lipid molecules, we apply

$$q_{\mathrm{L}}^\dagger(\mathbf{r}, s = N_{\mathrm{T}}^-) = [q_{\mathrm{L}}^\dagger(\mathbf{r}, s = N_{\mathrm{T}}^+)]^2 \tag{28}$$

$$q_{\mathrm{L}}(\mathbf{r}, s = N_{\mathrm{T}}^+) = q_{\mathrm{L}}(\mathbf{r}, s = N_{\mathrm{T}}^-)[q_{\mathrm{L}}^\dagger(\mathbf{r}, s = N_{\mathrm{T}}^+)] \tag{29}$$

In order to solve for $q_j(\mathbf{r}, s)$ and $q_j^\dagger(\mathbf{r}, s)$, we first determine $q_j^\dagger(\mathbf{r}, s)$ and then subsequently use it via eqs 27 and 29 to determine $q_j(\mathbf{r}, s)$. We assume no flux boundary conditions ($\nabla q_j = 0$) at the $r = 0$ and $r = r_\infty$ while we use periodic boundary conditions in the z-direction. We employed an alternating-direction implicit scheme[55] to solve the partial differential equations for $q_j(\mathbf{r},s)$ and $q_j^\dagger(\mathbf{r},s)$ in eqs 22 and 25 respectively. The spatial dimensions of our system are resolved on a mesh size of $\delta r = \delta z = 1/8R_g$ and the contour coordinate, s, is resolved on a mesh size of $\delta s = (N_{\mathrm{H}} + N_{\mathrm{T}})/64$.

A. Self-Consistent Equations

The self-consistent equations are found as the saddle point of eq 7 with respect to the fields $\varphi_i(\mathbf{r})$ (where i = $\mathrm{P_{NH}}$, $\mathrm{P_{NH_2}}$, G, H, T, $\mathrm{Na^+}$, $\mathrm{Cl^-}$, $\mathrm{H^+}$, $\mathrm{OH^-}$, and S), α, $w_i(\mathbf{r})$, and $\Phi(\mathbf{r})$. Such a procedure yields:[42]

$$w_{\mathrm{P}_j} = \zeta\left(\sum_{k=\mathrm{P,G,L,S}}\varphi_k - 1\right) - \frac{\epsilon_{\mathrm{PG}}}{2\rho_0}|\nabla\Phi|^2 + \alpha_{\mathrm{P}_j}\ln\left[\frac{1-f_j}{1-f_{\mathrm{b},j}}\right] - \alpha_{\mathrm{P}_j} \tag{30}$$

$$w_{\mathrm{G}}(\mathbf{r}) = \zeta\left(\sum_{k=\mathrm{P,G,L,S}}^{\max}\varphi_k - 1\right) - \frac{\epsilon_{\mathrm{PG}}}{2\rho_0}|\nabla\Phi|^2 \tag{31}$$

dx.doi.org/10.1021/jp4053049 | J. Phys. Chem. B 2013, 117, 9806−9820

$$w_H(\mathbf{r}) = \chi_{HT}\varphi_T + \chi_{HS}\varphi_S + \zeta\Big(\sum_{k=P,G,L,S}^{max}\varphi_k - 1\Big) + \kappa_H\nabla^2\varphi_H - \frac{\epsilon_H}{2\rho_0}|\nabla\Phi|^2 + z_H\alpha_H\Phi \quad (32)$$

$$w_T(\mathbf{r}) = \chi_{HT}\varphi_H + \chi_{TS}\varphi_S + \zeta\Big(\sum_{k=P,G,L,S}^{max}\varphi_k - 1\Big) + \kappa_T\nabla^2\varphi_T - \frac{\epsilon_T}{2\rho_0}|\nabla\Phi|^2 \quad (33)$$

$$w_S(\mathbf{r}) = \chi_{HS}\varphi_H + \chi_{TS}\varphi_T + \zeta\Big(\sum_{k=P,G,L,S}^{max}\varphi_k - 1\Big) - \frac{\epsilon_S}{2\rho_0}|\nabla\Phi|^2 \quad (34)$$

$$-\nabla\cdot(\epsilon\nabla\Phi) = \rho_0\sum_{j=NH,NH_2} z_{P_jH^+}\alpha_P f_j\varphi_{P_jH^+} + z_H\alpha_H\varphi_H + \sum_{i=ions} z_i\varphi_i \quad (35)$$

and

$$f_j = \frac{1}{1 + 10^{pK_{b,P_j} - pOH}\exp(-z_{OH}\Phi)} \quad (36)$$

In the above, z_i represents the charge valency of the i^{th} species and

$$\varphi_{P_{NH}} = \frac{1}{VQ_{PG}}\sum_{i=0}^{g-1}\Omega_i\int_{ni}^{n(i+1)} ds q_{PG}(s)q_{PG}^{\dagger}(s) \quad (37)$$

$$\varphi_{P_{NH_2}} = \frac{1}{VQ_{PG}}\Omega_g\int_{n(g-1)}^{ng} ds q_{PG}(s)q_{PG}^{\dagger}(s) \quad (38)$$

$$\varphi_G = \frac{1}{VQ_{PG}}\Omega_g\int_{ng}^{ng+N_G} ds q_{PG}(s)q_{PG}^{\dagger}(s) \quad (39)$$

$$\varphi_H = \int_0^{N_H} ds q_L(s)q_L^{\dagger}(s) \quad (40)$$

$$\varphi_L = \int_{N_H}^{N_T+N_H} ds q_L(s)q_L^{\dagger}(s) \quad (41)$$

$$\varphi_S = \exp[-\beta\mu_S]\exp[-w_S] \quad (42)$$

and

$$\varphi_{ion} = \exp[-\beta\mu_{ion}^{o}]\exp[-z_{ion}\Phi] \quad (43)$$

where v_j is the volume of a j^{th} molecule and Ω_i is the number of branches in the i^{th} generation.

To obtain $\Phi(\mathbf{r})$, we solve the Poisson-Boltzmann (PB) equation (eq 35) assuming no flux in the radial directions ($\nabla\Phi = 0$) at $r = 0$ and $r = r_\infty$ and periodic boundary conditions in the z-direction. For our simulation cell, we used a size of $15R_g$ for the cylinder radius and $40R_g$ for the cylinder height.

AUTHOR INFORMATION

Corresponding Author

*E-mail: venkat@che.utexas.edu.

Notes

The authors declare no competing financial interest.

ACKNOWLEDGMENTS

This work was supported in part by a grant from Robert A. Welch Foundation (grant F1599), the US Army Research Office under grant W911NF-07-1-0268, and National Science Foundation (DMR 1005739). The authors acknowledge the Texas Advanced Computing Center (TACC) at The University of Texas at Austin for providing computing resources that have contributed to the research results reported within this paper.

REFERENCES

(1) Mintzer, M. A.; Grinstaff, M. W. Biomedical Applications of Dendrimers: A Tutorial. *Chem. Soc. Rev.* **2011**, *40*, 173−190.

(2) KukowskaLatallo, J. F.; Bielinska, A. U.; Johnson, J.; Spindler, R.; Tomalia, D. A.; Baker, J. R. Efficient Transfer of Genetic Material into Mammalian Cells Using Starburst Polyamidoamine Dendrimers. *Proc. Natl. Acad. Sci. U.S.A.* **1996**, *93*, 4897−4902.

(3) Fant, K.; Eshjorner, E. K.; Jenkins, A.; Grossel, M. C.; Lincoln, P.; Norden, B. Effects of PEGylation and Acetylation of PAMAM Dendrimers on DNA Binding, Cytotoxicity and in Vitro Transfection Efficiency. *Mol. Pharmaceutics* **2010**, *7*, 1734−1746.

(4) Hong, S. P.; Bielinska, A. U.; Mecke, A.; Keszler, B.; Beals, J. L.; Shi, X. Y.; Balogh, L.; Orr, B. G.; Baker, J. R.; Holl, M. M. B. Interaction of Poly(amidoamine) Dendrimers with Supported Lipid Bilayers and Cells: Hole Formation and the Relation to Transport. *Bioconjugate Chem.* **2004**, *15*, 774−782.

(5) Mecke, A.; Majoros, I. J.; Patri, A. K.; Baker, J. R.; Holl, M. M. B.; Orr, B. G. Lipid Bilayer Disruption by Polycationic Polymers: The Roles of Size and Chemical Functional Group. *Langmuir* **2005**, *21*, 10348−10354.

(6) Kelly, C. V.; Liroff, M. G.; Triplett, L. D.; Leroueil, P. R.; Mullen, D. G.; Wallace, J. M.; Meshinchi, S.; Baker, J. R.; Orr, B. G.; Holl, M. M. B. Stoichiometry and Structure of Poly(amidoamine) Dendrimer-Lipid Complexes. *ACS Nano* **2009**, *3*, 1886−1896.

(7) Leroueil, P. R.; Berry, S. A.; Duthie, K.; Han, G.; Rotello, V. M.; McNerny, D. Q.; Baker, J. R.; Orr, B. G.; Holl, M. M. B. Wide Varieties of Cationic Nanoparticles Induce Defects in Supported Lipid Bilayers. *Nano Lett.* **2008**, *8*, 420−424.

(8) Jevprasesphant, R.; Penny, J.; Jalal, R.; Attwood, D.; McKeown, N. B.; D'Emanuele, A. The Influence of Surface Modification on the Cytotoxicity of PAMAM Dendrimers. *Int. J. Pharm.* **2003**, *252*, 263−266.

(9) Wang, W.; Xiong, W.; Wan, J. L.; Sun, X. H.; Xu, H. B.; Yang, X. L. The Decrease of PAMAM Dendrimer-Induced Cytotoxicity by PEGylation via Attenuation of Oxidative Stress. *Nanotechnology* **2009**, *20*, 105103.

(10) Lee, H.; Larson, R. Molecular Dynamics Simulations of PAMAM Dendrimer-Induced Pore Formation in DPPC Bilayers Using a Coarse Grained Model. *Abstr. Pap. Am. Chem. Soc.* **2006**, *232*, 342−342.

(11) Lee, H.; Larson, R. G. Coarse-Grained Molecular Dynamics Studies of the Concentration and Size Dependence of Fifth- and Seventh-Generation PAMAM Dendrimers on Pore Formation in DMPC Bilayer. *J. Phys. Chem. B* **2008**, *112*, 7778−7784.

(12) Lee, H.; Larson, R. G. Lipid Bilayer Curvature and Pore Formation Induced by Charged Linear Polymers and Dendrimers: The Effect of Molecular Shape. *J. Phys. Chem. B* **2008**, *112*, 12279−12285.

(13) Kelly, C. V.; Leroueil, P. R.; Nett, E. K.; Wereszczynski, J. M.; Baker, J. R.; Orr, B. G.; Holl, M. M. B.; Andricioaei, I. Poly(amidoamine) Dendrimers on Lipid Bilayers I: Free Energy and Conformation of Binding. *J. Phys. Chem. B* **2008**, *112*, 9337−9345.

(14) Kelly, C. V.; Leroueil, P. R.; Orr, B. G.; Holl, M. M. B.; Andricioaei, I. Poly(amidoamine) Dendrimers on Lipid Bilayers II: Effects of Bilayer Phase and Dendrimer Termination. *J. Phys. Chem. B* **2008**, *112*, 9346−9353.

(15) Yan, L. T.; Yu, X. B. Charged Dendrimers on Lipid Bilayer Membranes: Insight through Dissipative Particle Dynamics Simulations. *Macromolecules* **2009**, *42*, 6277−6283.
(16) Yan, L. T.; Yu, X. B. Enhanced Permeability of Charged Dendrimers across Tense Lipid Bilayer Membranes. *ACS Nano* **2009**, *3*, 2171−2176.
(17) Ainalem, M. L.; Campbell, R. A.; Khalid, S.; Gillams, R. J.; Rennie, A. R.; Nylander, T. On the Ability of PAMAM Dendrimers and Dendrimer/DNA Aggregates to Penetrate POPC Model Biomembranes. *J. Phys. Chem. B* **2010**, *114*, 7229−7244.
(18) Lin, X. B.; Li, Y.; Gu, N. Molecular Dynamics Simulations of the Interactions of Charge-Neutral PAMAM Dendrimers with Pulmonary Surfactant. *Soft Matter* **2011**, *7*, 3882−3888.
(19) Lee, H.; Larson, R. G. Membrane Pore Formation Induced by Acetylated and Polyethylene Glycol-Conjugated Polyamidoamine Dendrimers. *J. Phys. Chem. C* **2011**, *115*, 5316−5322.
(20) Tian, W. D.; Ma, Y. Q. Insights into the Endosomal Escape Mechanism via Investigation of Dendrimer−Membrane Interactions. *Soft Matter* **2012**, *8*, 6378−6384.
(21) Ginzburg, V. V.; Balijepailli, S. Modeling the Thermodynamics of the Interaction of Nanoparticles with Cell Membranes. *Nano Lett.* **2007**, *7*, 3716−3722.
(22) Ting, C. L.; Wang, Z. G. Interactions of a Charged Nanoparticle with a Lipid Membrane: Implications for Gene Delivery. *Biophys. J.* **2011**, *100*, 1288−1297.
(23) Ting, C. L.; Wang, Z. G. Minimum Free Energy Paths for a Nanoparticle Crossing the Lipid Membrane. *Soft Matter* **2012**, *8*, 12066−12071.
(24) Ding, H. M.; Tian, W. D.; Ma, Y. Q. Designing Nanoparticle Translocation through Membranes by Computer Simulations. *ACS Nano* **2012**, *6*, 1230−1238.
(25) Li, Y.; Gu, N. Thermodynamics of Charged Nanoparticle Adsorption on Charge-Neutral Membranes: A Simulation Study. *J. Phys. Chem. B* **2010**, *114*, 2749−2754.
(26) Nandy, B.; Maiti, P. K. DNA Compaction by a Dendrimer. *J. Phys. Chem. B* **2011**, *115*, 217−230.
(27) Lewis, T.; Ganesan, V. Mean-Field Modeling of the Encapsulation of Weakly Acidic Molecules in Polyelectrolyte Dendrimers. *J. Phys. Chem. B* **2012**, *116*, 8269−8281.
(28) Lewis, T.; Ganesan, V. Conjugation of Polybasic Dendrimers with Neutral Grafts: Effect on Conformation and Encapsulation of Acidic Drugs. *Soft Matter* **2012**, *8*, 11817−11830.
(29) Lewis, T.; Pryamitsyn, V.; Ganesan, V. Mean Field Theory of Charged Dendrimer Molecules. *J. Chem. Phys.* **2011**, *135*, 204902.
(30) Lewis, T.; Pandav, G.; Omar, A.; Ganesan, V. Complexation between Weakly Basic Dendrimers and Linear Polyelectrolytes: Effects of Grafts, Chain Stiffness, and pOH. *Soft Matter* **2013**, *9* (29), 6955−6969.
(31) Wu, B.; Chen, W. R.; Egami, T.; Li, X.; Liu, Y.; Wang, Y. M.; Do, C.; Porcar, L.; Hong, K. L.; Liu, L.; Smith, G. S.; Smith, S. C. Molecular Dynamics and Neutron Scattering Study of the Dependence of Polyelectrolyte Dendrimer Conformation on Counterion Behavior. *J. Chem. Phys.* **2012**, *137*, 064902.
(32) Behr, J. P. The Proton Sponge: A Trick to Enter Cells the Viruses Did Not Exploit. *Chimia* **1997**, *51*, 34−36.
(33) Sonawane, N. D.; Szoka, F. C.; Verkman, A. S. Chloride Accumulation and Swelling in Endosomes Enhances DNA Transfer by Polyamine-DNA Polyplexes. *J. Biol. Chem.* **2003**, *278*, 44826−44831.
(34) Yang, S.; May, S. Release of Cationic Polymer-DNA Complexes from the Endosome: A Theoretical Investigation of the Proton Sponge Hypothesis. *J. Chem. Phys.* **2008**, *129*, 185105.
(35) Luo, D.; Haverstick, K.; Belcheva, N.; Han, E.; Saltzman, W. M. Poly(ethylene glycol)-Conjugated PAMAM Dendrimer for Biocompatible, High-Efficiency DNA Delivery. *Macromolecules* **2002**, *35*, 3456−3462.
(36) Hedden, R. C.; Bauer, B. J. Structure and Dimensions of PAMAM/PEG Dendrimer-Star Polymers. *Macromolecules* **2003**, *36*, 1829−1835.
(37) Tomalia, D. A.; Naylor, A. M.; Goddard, W. A. Starburst Dendrimers - Molecular-Level Control of Size, Shape, Surface-Chemistry, Topology, and Flexibility from Atoms to Macroscopic Matter. *Angew. Chem., Int. Ed. Engl.* **1990**, *29*, 138−175.
(38) Carbone, P.; Negri, F.; Muller-Plathe, F. A Coarse-Grained Model for Polyphenylene Dendrimers: Switching and Backfolding of Planar Three-Fold Core Dendrimers. *Macromolecules* **2007**, *40*, 7044−7055.
(39) Carbone, P.; Muller-Plathe, F. Molecular Dynamics Simulations of Polyaminoamide (PAMAM) Dendrimer Aggregates: Molecular Shape, Hydrogen Bonds and Local Dynamics. *Soft Matter* **2009**, *5*, 2638−2647.
(40) Huissmann, S.; Wynveen, A.; Likos, C. N.; Blaak, R. The Effects of pH, Salt and Bond Stiffness on Charged Dendrimers. *J. Phys.: Condens. Matter* **2010**, *22*, 232101.
(41) Wolterink, J. K.; van Male, J.; Daoud, M.; Borisov, O. V. Starburst Polyelectrolytes: Scaling and Self-Consistent-Field Theory. *Macromolecules* **2003**, *36*, 6624−6631.
(42) Fredrickson, G. *The Equilibrium Theory of Inhomogeneous Polymers*; Oxford University Press: New York, 2006.
(43) Tanis, I.; Karatasos, K. Molecular Dynamics Simulations of Polyamidoamine Dendrimers and Their Complexes with Linear Poly(ethylene oxide) at Different pH Conditions: Static Properties and Hydrogen Bonding. *Phys. Chem. Chem. Phys.* **2009**, *11*, 10017−10028.
(44) Nap, R.; Gong, P.; Szleifer, I. Weak Polyelectrolytes Tethered to Surfaces: Effect of Geometry, Acid-Base Equilibrium and Electrical Permittivity. *J. Polym. Sci., Part B: Polym. Phys.* **2006**, *44*, 2638−2662.
(45) Gong, P.; Genzer, J.; Szleifer, I. Phase Behavior and Charge Regulation of Weak Polyelectrolyte Grafted Layers. *Phys. Rev. Lett.* **2007**, *98*, 018302.
(46) Uline, M. J.; Rabin, Y.; Szleifer, I. Effects of the Salt Concentration on Charge Regulation in Tethered Polyacid Monolayers. *Langmuir* **2011**, *27*, 4679−4689.
(47) Witte, K. N.; Kim, S.; Won, Y. Y. Self-Consistent Field Theory Study of the Effect of Grafting Density on the Height of a Weak Polyelectrolyte Brush. *J. Phys. Chem. B* **2009**, *113*, 11076−11084.
(48) Hur, J.; Witte, K. N.; Sun, W.; Won, Y. Y. On the Origins of the Salt-Concentration-Dependent Instability and Lateral Nanoscale Heterogeneities of Weak Polyelectrolyte Brushes: Gradient Brush Experiment and Flory-Type Theoretical Analysis. *Langmuir* **2010**, *26*, 2021−2034.
(49) Niu, Y. H.; Sun, L.; Crooks, R. A. Determination of the Intrinsic Proton Binding Constants for Poly(amidoamine) Dendrimers via Potentiometric pH Titration. *Macromolecules* **2003**, *36*, 5725−5731.
(50) Nagle, J. F.; Tristram-Nagle, S. Structure of Lipid Bilayers. *Biochim. Biophys. Acta, Rev. Biomembr.* **2000**, *1469*, 159−195.
(51) Olbrich, K.; Rawicz, W.; Needham, D.; Evans, E. Water Permeability and Mechanical Strength of Polyunsaturated Lipid Bilayers. *Biophys. J.* **2000**, *79*, 321−327.
(52) Smith, P. E. S.; Brender, J. R.; Durr, U. H. N.; Xu, J. D.; Mullen, D. G.; Holl, M. M. B.; Ramamoorthy, A. Solid-State NMR Reveals the Hydrophobic-Core Location of Poly(amidoamine) Dendrimers in Biomembranes. *J. Am. Chem. Soc.* **2010**, *132*, 8087−8097.
(53) Jevprasesphant, R.; Penny, J.; Attwood, D.; D'Emanuele, A. Transport of Dendrimer Nanocarriers through Epithelial Cells via the Transcellular Route. *J. Controlled Release* **2004**, *97*, 259−267.
(54) Grason, G. M.; Kamien, R. D. Self-Consistent Field Theory of Multiply Branched Block Copolymer Melts. *Phys. Rev. E* **2005**, *71*, 051801.
(55) Press, W. H.; Teukolsky, S. A.; Vetterling, W. T.; Flannery, B. P. *Numerical Recipies: The Art of Scientific Computing*; Cambridge University Press: Cambridge, U.K., 2007.